Journal of Quantitative Spectroscopy & Radiative Transfer 213 (2018) 119–132

Contents lists available at ScienceDirect

Journal of Quantitative Spectroscopy & Radiative Transfer

journal homepage: www.elsevier.com/locate/jqsrt

FT-IR measurements of cold propene (C_3H_6) cross-sections at temperatures between 150 and 299 K

Keeyoon Sung[a,*], Geoffrey C. Toon[a], Brian J. Drouin[a], Arlan W. Mantz[b], Mary Ann H. Smith[c]

[a] Jet Propulsion Laboratory, California Institute of Technology, 4800 Oak Grove Dr., Pasadena, CA 91109, USA
[b] Department of Physics, Astronomy and Geophysics, Connecticut College, New London, CT 06320, USA
[c] Science Directorate, NASA Langley Research Center, Hampton, VA 23681, USA

ARTICLE INFO

Article history:
Received 25 September 2017
Revised 25 January 2018
Accepted 13 March 2018
Available online 17 March 2018

ABSTRACT

In support of infrared remote sensing of Titan, we present temperature dependent cross-sections of propene (C_3H_6; $CH_2{=}CH{-}CH_3$; propylene) measured in the laboratory. A total of 27 high-resolution (up to 0.0022 cm^{-1}) spectra of pure C_3H_6 and mixtures of C_3H_6 with N_2 were obtained at 150–299 K in the 650–1534 cm^{-1} (6.5–15.4 µm) region. A custom-designed cold cell was used, which was configured with an active temperature control and could be integrated to a Fourier-transform spectrometer (Bruker 125HR) at the Jet Propulsion Laboratory. The observed C_3H_6 spectral features include its strong ν_{19} band bearing the most prominent Q-branch peak at 912 cm^{-1} and three other strong bands: ν_{18}, ν_{16} and ν_7 centered near 991, 1443, and 1459 cm^{-1}, respectively. In addition, we have generated empirical pseudoline lists (PLLs) in HITRAN-format, in the two separate spectral regions, which are Region I: 800–1100 and Region II: 1340–1524 cm^{-1}. The PLLs of C_3H_6 consists of spectroscopic line parameters (including line intensities and effective lower state energies) for all the individual pseudoline positions. The pseudoline parameters were determined by fitting 27 laboratory spectra of pure and N_2-broadened propene simultaneously in the selected regions. A newly derived partition function was adopted in the line-by-line radiative transfer calculations. Based on the pseudoline intensities, the total integrated intensities in the 800–1120 and 1320–1524cm^{-1} regions were measured to be $8.79(47)\times 10^{-18}$ and $3.06(21)\times 10^{-18} cm^{-1}/(molecule\ cm^{-2})$ at 296 K, respectively. These values are found to be in a good agreement with the recent measurement made at KAUST at room temperature, but they are significantly lower than those reported by one of the most extensive previous studies at the Pacific Northwest National Laboratory (PNNL). Finally, the two PLLs are submitted as electronic supplements and are also available from the website, https://mark4sun.jpl.nasa.gov/pseudo.html.

1. Introduction

Propene was discovered in the stratosphere of Titan [1] well after the other C_3-hydrocarbons propyne (C_3H_4) and propane (C_3H_8), bearing a triple bond and single bond, respectively, were observed by Voyager/IRIS [2,3] more than three decades ago. Thus, propene became the first unsaturated C_3-hydrocarbon species bearing a double bond detected in the stratosphere of Titan by Cassini/CIRS (Composite Infrared Spectrometer) [1]. In fact, Nixon et al. [4] had already identified an excess emission feature at 912 cm^{-1} in the residual spectra of Cassini/CIRS as belonging to propene, based on the PNNL low-resolution cross-sections of C_3H_6 measured at warmer temperatures (*i.e.*, 278, 298, and 323 K) [5]. However, some other nearby excess emission features had remained persistent when the PNNL propane cross-sections [5] were used in the radiative transfer calculations. The use of high-resolution measurements of propane (C_3H_8) cross-sections measured at cold temperatures (down to 150 K) relevant to the Titan's stratosphere [6] has enabled the definitive identification of propene (C_3H_6) by accounting for other excess emission features in the vicinity of the propene features in the CIRS residual spectra. The propene detection reported by Nixon et al. [1] demonstrates the importance of using reliable spectroscopic reference data obtained at the right temperature conditions. The detection of propene in Titan's stratosphere has prompted its high-resolution spectroscopic study at cold temperatures relevant to Titan, the results of which would enable better quantitative observation of the new species as well as making visible in the residuals any features from other species yet to

---

* Corresponding author.
E-mail address: ksung@jpl.nasa.gov (K. Sung).

https://doi.org/10.1016/j.jqsrt.2018.03.011

be identified. Therefore, we have measured high-resolution cross-sections of propene in the 7–15 μm region by analyzing a series of Fourier transform spectra of pure propene and mixtures of propene with N_2, recorded over the 150–299 K temperature range.

Propene (propylene, methyl ethylene) is an unsaturated organic compound bearing one double bond ($H_3C{-}CH{=}CH_2$), also sharing the chemical formula, C_3H_6, with its structural isomer, cyclopropane. It is the second simplest member of the alkene class of hydrocarbons, following ethene (C_2H_4). Along with ethene, propene is an important intermediate species in many hydrocarbon reactions, becoming an indispensable compound in petrochemical industries and industrial applications, such as for the synthesis of polypropylene [7–10]. It is also released into the Earth's atmosphere by vegetation and by fermentation processes as well as from biomass burning [11–13].

Propene was detected in interstellar space a decade ago, in the Taurus Molecular Cloud (TMC-1) [14]. The observation of propene in a rarified and cold cloud has raised an important question about its production channels. In interstellar space, it has been suggested that grain surface reactions (*e.g.* successive hydrogenations from C_3 or C_3H_2 on grain surfaces) play a significant role in the synthesis of gas-phase propene [15–17]. Several other C_3-hydrocarbons (*e.g.* C_3, C_3H, C_3H_2, C_3H_4) have also been detected in interstellar space and/or in carbon-rich circumstellar envelopes [18–24].

Propene plays a key role in the evolution of the chemical constituents of Titan's atmosphere. It was detected in the ionosphere of Titan by Cassini's Ion Neutral Mass Spectrometer (INMS) [25–27]. It was predicted to be present in Titan's lower atmosphere [28,29] where photo-induced processes dominate the neutral chemistry [30–33]. In particular, Krasnopolsky [34] studied C_3-hydrocarbons in detail in his updated model of the photochemistry of the Titan atmosphere, incorporating 23 reactions involving the chemistry of propene, which was able to reproduce very well the observed propene abundances available from the Cassini INMS and CIRS instruments for both in the ionosphere and stratosphere of Titan, respectively. Furthermore, an extended photochemical model for exoplanets has predicted propene to be one of the hydrocarbons expected in those atmospheres [35].

2. Spectroscopy overview of propene in the mid-infrared region

As an asymmetric methyl internal rotor [36], propene has permanent dipole moments, $\mu_a = 0.360$ and $\mu_b = 0.05$ Debye [37]; this allows rotational transitions to be studied at microwave and millimeter wavelengths [18] and facilitates its observation in interstellar space [14]. Propene has a potential barrier $V_3 = 692.6$ cm^{-1} [18] against the torsional motion of the CH_3 group (in contrast, for CH_3OH, the three-fold potential barrier is only $V_3 = 373$ cm^{-1}). Therefore, a very small *A*/*E* splitting (0.0013 cm^{-1}) is expected for torsional sub-states of propene in the ground vibrational and non-torsional vibrationally excited states. Resolving these splittings would require very high-resolution ($<$0.0013 cm^{-1}) beyond the capability of our instrument in consideration of signal-to-noise ratios.

Propene has 21 fundamental vibrational modes, listed in Table 1. All are infrared active, and three of them fall below $\sim$700 cm^{-1}. The low energy modes give rise to numerous observable overtone, combination and hot bands throughout the infrared spectrum of this molecule. The low-lying states generate rich and dense spectral features, whose transitions are mostly unresolved even in Doppler-limited spectra recorded at room temperature. Lafferty et al. [36] analyzed two propene bands, ν_{18} and ν_{19}, in the 10 – 11 μm region using jet-cooled FTIR spectra recorded at the rotational temperature of 80 K, in which the torsional hot band features are effectively suppressed. They investigated the fine structure of these bands and obtained the approximate principal rotational constants as well as the band origins, but no line intensities or cross-sections were reported. In the absence of any other high-resolution line-by-line studies of propene in the infrared, relevant laboratory spectroscopic measurements of propene cross-sections at high spectral resolution are still needed, especially at cold temperatures. This work supports spectroscopic observations of Titan's atmosphere in the infrared region, 7–15 μm, covered by various NASA space missions and ground-based observatories, such as Voyager/IRIS [2], ISO/SWS [41], IRTF/TEXES [42], Cassini/CIRS [43] and the upcoming JWST [44,45].

Table 1
Fundamental bands of propene (band centers in cm^{-1}).[a]

ν_1 (3091.62)	ν_8 (1420)	ν_{15} (2954.30)
ν_2 (3015)	ν_9 (1377.94)[b]	ν_{16} (1442.71)[b]
ν_3 (2991.03)	ν_{10} (1297.86)[b]	ν_{17} (1045.20)[c]
ν_4 (2973)	ν_{11} (1170.04)[b]	ν_{18} (990.7761)[d]
ν_5 (2931.46)	ν_{12} (935.67)[c]	ν_{19} (912.6677)[d]
ν_6 (1653.18)	ν_{13} (919.29)[c]	ν_{20} (576.27)
ν_7 (1458.5)[e]	ν_{14} (426.02)	ν_{21} (188)

[a] Adopted from [52] https://www.astro.washington.edu/spectra; Demaison and Rudolph [10], but keeping the values more consistent with the present study.
[b] Adopted from Es-Sebbar et al. [38].
[c] from Ainetschian et al. [39].
[d] from Lafferty et al. [36].
[e] from Silvi et al. [40].

Substantial features from the fundamental bands (listed in Table 1) and their combination bands with its lowest-lying torsional band would be still present in the cold atmosphere of Titan and even get stronger for low-J transition near the band center contributing to its atmospheric opacity. Furthermore, diverse saturated hydrocarbons are expected in the Titan atmosphere, produced *via* chain reactions from photochemistry initiated by CH_4 photolysis in the upper atmosphere [46,47], (This results in an observed spectrum densely populated with spectroscopic features particularly in the mid-infrared region where most molecules have strong fundamental bands. As discussed by Sung et al. [6], the 7–15 μm spectral region in the CIRS spectra contains features from many other important hydrocarbons in the vicinity of the propene features; C_2H_6 (ν_9) at 821 cm^{-1} near the ν_{19} band of propene, C_2H_6 (ν_6) at 1379.2 cm^{-1} near the ν_9 band of propene, C_2H_6 (ν_8) at 1468 cm^{-1} and $C_2H_6(\nu_{11})$ at 1469 cm^{-1} near the ν_7 band of propene [4] and CH_3D at 1158 cm^{-1} near the ν_{11} band of propene. Therefore, the role of high-resolution spectroscopic input to the atmospheric opacity calculations is even more crucial to accurate interpretation of the observed Titan atmospheric spectra and identification of possible new molecules throughout the 7–15 μm region.

The major absorption features of propene in the mid-infrared can be characterized by a few strong bands, which include the ν_{19} band at 912 cm^{-1}, ν_{18} band at 991 cm^{-1}, ν_{16} and ν_7 bands in the 1460 cm^{-1} region. The rovibrational features of propene are seen substantially smeared out in the broad-band FT-IR spectra from this work. A 'continuum-like absorption' feature may be generated by the aggregated contribution from numerous hot bands and weak features from possible combination bands involving low-lying states. They could be misinterpreted as arising from 'ice/aerosol/haze' if not properly accounted-for in the spectroscopic analysis. However, detailed characterization of individual transitions and global fitting through Hamiltonian modeling is very challenging for propene. Thus, empirical absorption coefficients or cross-sections must be used until line-by-line spectroscopic measurements and model predictions become available in the public databases, such as HITRAN [48–50] and GEISA [53,54].

Early work focused on the molecular structure or torsional splitting of propene [10,36,39,55,56] but provided no cross-sections. Measurements of cross-sections have become available from NIST (NIST Chem Webbook, http://webbook.nist.gov/chemistry) at room temperatures. The Pacific Northwest National Lab (PNNL) catalog ([5]; https://secure2.pnl.gov/nsd/nsd.nsf/Welcome) carries a very extensive set of absorption coefficients data including those of C_3H_6, all of which were obtained at relatively *warm* temperatures (278, 298, 323 K) with the gas samples in mixtures with N_2 at one bar [5]. More recently, measurements of propene cross-sections were reported at elevated temperatures (296 – 460 K) with a very broad spectral coverage from 400 – 6500 cm^{-1} [38] and at 298–700 K in the 3 µm region [57].

In this work, we have measured high-resolution cross-sections of pure and N_2-broadened propene at various temperatures between 150 and 299 K to provide more representative laboratory input for Titan atmospheric studies. On the top of the measurements at the cold temperature, such a high resolution (up to 0.0022 cm^{-1}) broad-band FT-IR spectroscopy will provide the best band-to-band consistency for the Cassini/CIRS observation analysis, in addition to be able to capture the fine details in the absorption features, for instance, the sub-Q branches, $^{\Delta K_a}Q_J$ associated with individual values of the rotational quantum number *J*. Furthermore, the results from this work can be used in support of Solar System Science with the upcoming James Webb Space Telescope (JWST) for Titan [45], specifically for the JWST/MIRI (Mid Infrared Instrument) which will have a slightly better spectral resolution than the Cassini/CIRS instrument in the 7 µm region (*i.e.*, 0.4 cm^{-1} for MIRI *vs.* 0.5 cm^{-1} for CIRS). The higher resolution provides a better chance of detecting features due to weak bands and revealing new species that have not been discernable in the CIRS spectra because of too much overlap (*e.g.*, propane and propene at around 11 µm [1]).

It should be noted, however, that the compiled cross-sections have their own limitation; they should be measured at various combinations of sample pressures and temperatures covering the range of physical conditions relevant to the Titan atmosphere. In this work, we have taken an additional step to make our results more amenable to line-by-line calculations. We have generated a HITRAN-format list of pseudolines, which can be an effective alternative to true spectroscopic line parameters in radiative transfer calculations, as described in a later section.

3. Experimental details

We obtained a series of high-resolution absorption spectra of pure and N_2-broadened propene ($H_3C{-}CH{=}CH_2$) at temperatures from 297 to 150 K using a 20.38 cm long cold cell and a Fourier-transform spectrometer (FTS), Bruker IFS-125HR, at the Jet Propulsion Laboratory (JPL). A high purity (99%) gas sample of normal propene (*i.e.,* with no isotope-enrichment) from Sigma-Aldrich, Inc. and a research grade (99.9999%) N_2 were used in the spectral data acquisition with no further purification. We used a straight cold cell, which was developed at Connecticut College [58], and installed in the sample compartment of the Bruker IFS-125HR at JPL. Detailed characterization of the cold cell can be found in Sung et al. [59]. In particular, the cold cell has an excellent temperature control in the wide range of the temperatures down to 80 K with a temperature stability better than 0.01 K/h. The cold cell has become one of our primary optics in our laboratory, producing high quality data in our previous work [6,60–63]. The temperature accuracy of 0.1 K, as reported in Table 2, has also been previously characterized.

As is summarized in Table 2, the instrument was configured with a Globar lamp, a KBr beam splitter, and a LN_2-cooled HgCdTe (MCT) detector. An optical filter covering 650–1550 cm^{-1} was used to obtain the desired bandpass. The aperture diameter was set to be either 1.7 or 2.0 mm, depending on the spectral resolution. The optical paths in the Bruker FTS chambers were continuously evacuated to a pressure of ~10 mTorr to minimize the residual water content. As was described in [6], the sample pressures were continually monitored using three different Baratron pressure gauges with 0–10, 0–100 and 0–1000 Torr pressure ranges.

Table 2
Instrumental configuration of the Bruker IFS-125HR.

Spectral region	650–1550 cm^{-1}
Bands covered	ν_{19}, ν_{18}, ν_{17}, ν_9, ν_{16}, ν_7
Resolutions	0.0022–0.01 cm^{-1} (depending on sample pressures)
# of spectra	27 (4 pure and 23 N_2-broadened)
Aperture(dia.)	1.7, 2.0 mm
IR source	Globar
Beam splitter	KBr
Cell length	20.38 cm
Cell temperature	coolable down to ~77 K with accuracy of 0.1 K
Windows	ZnSe for the cell; KBr for the vacuum box (both wedged)
Detectors	HgCdTe (LN_2 cooled)
Sample	C_3H_6 (99%), N_2 (99.9999%)
FTS pressure	<10 mTorr

We have obtained a series of spectra of pure propene and its N_2-mixture in the wide temperature ranges (299–150 K), among which a total of 27 spectra were selected and analyzed in this work after careful assessment of the spectrum quality (*e.g. signal-to-noise ratio, S*/*N*, water interference, optical depth, and resolving power of the given spectral resolution). For decent optical depth at the desired experimental conditions, various combinations of total pressures and volume mixing ratios of C_3H_6 were selected. A summary of the experimental conditions for the spectra is provided in Table 3, sorted in decreasing order of the measurement temperatures. Interferograms of sample and background scans were collected and then Fourier-transformed individually to generate the spectra, which were coadded to enhance the S/N, which was better than 300 for most cases. Each propene spectrum was ratioed to its corresponding empty cell spectrum, producing transmittance spectra which were then analyzed for the absorption cross-sections and the pseudoline generation.

The sample temperatures were monitored using a silicon diode sensor attached to the cell body at a point farthest away from the control heater. The measurement temperature range was chosen to support spectroscopic observations of Titan's stratosphere (250–140 K) and Earth's troposphere (296–190 K). The measurement pressures were chosen to avoid any possible condensation within the cell.

For example, at 150 K, the saturation vapor pressure of propene is approximately 3 Torr (4 hPa) (CRC Book), [64], which is in principle the maximum sample pressure that one can put in the cell without taking a risk of condensation. So the actual C_3H_6 sample pressures in our cell were always lower than the saturation vapor pressure by a factor of three or so in order to avoid any possible condensation on the cold windows.

The spectral resolutions were adaptively selected to match Voigt line width estimates at the given sample pressures and temperatures for the N_2-broadened spectra, which can be approximated to be $\surd(\gamma_D{}^2+\gamma_L{}^2)$, where γ_D = Doppler width at 11µm, γ_L= Lorentz width assumed to be 0.12 cm^{-1}/atm [60] as described in more detail in Section 5. Empty cell spectra were obtained at the same spectral resolutions as those of their gas sample counterparts to facilitate a point-by-point spectrum ratio. The system showed excellent photometric and temperature stability as was noted earlier [59]. The drift from the true 100% transmission (*i.e.*, continuum level) in the ratio spectra was observed to be less than 0.5% for the spectra at a given temperature. A typical example of N_2-broadened spectra of C_3H_6 is presented in Fig. 2, in which the strongest ab-

Table 3
Experimental conditions of the pure and N_2-broadened C_3H_6 spectra analyzed in this work for two spectral regions, Region I and II (*See text*).

#	Spectra	800–1524 cm^{-1}			Resolution[b] (cm^{-1})
		T (K)	P_t[a] (Torr)	P_s[a] (Torr)	
Pure sample spectra					
1	B0132.1a	298.9(5)	9.657	9.657	0.0022
2	B0132.5c	270.1(1)	9.938	9.938	0.0022
3	B0132.4a	230.1(1)	8.238	8.238	0.0022
4	B0132.3c	190.2(1)	7.479[&]	7.479	0.0022
N_2-broadened spectra					
5	B0117.2a	296.0(5)	85.31	0.910	0.0044
6	B0132.1c	299.1(5)	109.8	4.598	0.01
7	B0132.1d	299.2(5)	34.70	1.453	0.005
8	B0164.1b	297.0(5)	888.0	2.000	0.062
9	B0164.1c	297.1(5)	888.0	2.000	0.01
10	B0164.2c	297.5(5)	759.4	2.881	0.02
11	B0164.3c	296.6(5)	113.6	5.606	0.01
12	B0164.3e	295.5(5)	762.6	4.606	0.04
13	B0132.5a	270.1(1)	101.8	2.986	0.01
14	B0132.5b	270.1(1)	48.54	1.424	0.0067
15	B0132.5d	270.1(1)	102.9	9.938	0.01
16	B0132.5e	270.1(1)	48.11	4.646	0.0067
17	B0164.4b	270.0(1)	690.8	3.869	0.042
18	B0132.4b	230.1(1)	107.3	8.210	0.012
19	B0132.4c	230.1(1)	41.77	3.199	0.0067
20	B0132.4d	230.1(1)	99.95	0.999	0.01
21	B0164.5b	230.0(1)	590.1	3.260	0.042
22	B0132.3a	190.2(1)	98.23[&]	1.000	0.01
23	B0132.3d	190.2(1)	101.4[&]	7.201	0.01
24	B0164.6b	190.0(1)	497.1	2.000	0.042
25	B0117.1b	150.2(1)	37.43	0.404	0.0044
26	B0132.2b	150.3(1)	102.5	0.993	0.01
27	B0164.7b	150.0(1)	394.5	1.044	0.042

Notes: P_t = total pressure; P_s = C_3H_6 partial pressure; 1 atm = 1013 mb = 760 Torr.

[a] Uncertainty in the sample pressures is 1–5% for the spectra marked by [&] due to a small leak around the window assembly. For all other spectra, the uncertainties are better than 0.5% for the sample pressure readings.

[b] Spectral resolution was defined by 0.5/MOPD, where MOPD is Maximum Optical Path Difference (Note that the Bruker FTS resolution parameter is given by 0.9/MOPD).

sorption features are noted in two distinctive spectral regions, *i.e.*, Region I: 800–1100 cm^{-1} and Region II: 1340–1524 cm^{-1}.

The individual band features identified are ν_{19} at 912 cm^{-1}, ν_{18} at 991 cm^{-1}, and ν_{17} at 1045 cm^{-1} in Region I, and ν_9 at 1378 cm^{-1}, ν_{16} at 1443 cm^{-1}, and ν_7 at 1459 cm^{-1} in Region II. The bands ν_{10} and ν_{11} (centered at 1298 and 1170 cm^{-1}, respectively) were too weak to be measured in this work. Any contributions from the ν_{12} (935.7 cm^{-1}) and ν_{13} (919.3 cm^{-1}) bands were included in the cross section of Region I, although their features were not identifiable in our spectrum set, despite the prediction of their being as strong as the ν_9 band (1378 cm^{-1}) [65]. Pronounced features from the central Q-branches for each band are easily seen for most bands except for the ν_7 parallel band, while a very weak central Q-branch feature is seen for the ν_9 band. The ν_{19} band, which is the strongest fundamental band having a prominent Q-branch, was used to detect C_3H_6 in the Titan stratosphere [4]. Besides, there are many line-like features of the ${}^{\Delta Ka}Q_J$ sub-branches spread over each band. The crowded absorption features are efficiently broadened out by the cold N_2, as shown in Fig. 2 for the $C_3H_6 + N_2$ mixture spectra.

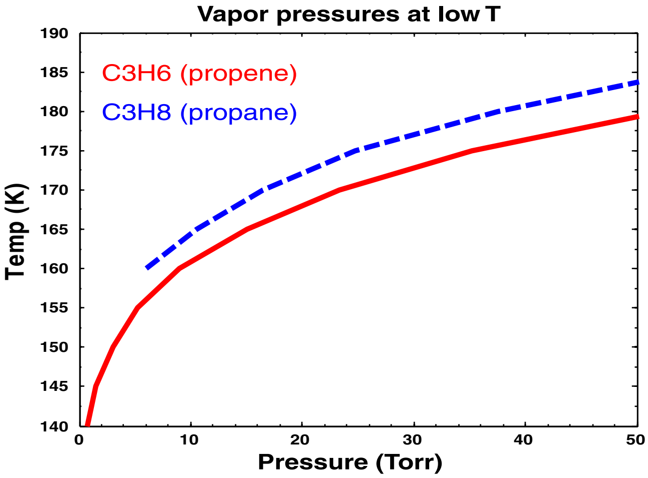

Fig. 1. Vapor pressure of C_3H_6 (solid line) adopted from CRC Book [64], compared to C_3H_8 (dashed line).

3. Cross-sections of propene (C_3H_6) in the 7–15 μm region at various cold temperatures

Since the two spectral regions, 800–1100 cm^{-1} and 1340–1524 cm^{-1}, appear to be very well isolated from the neighboring bands, their cold cross-sections were derived from the transmission spectra separately. As shown in the sample spectrum in Fig. 2, the 100% transmission level was observed to be very well defined (within 0.5%). All of the 27 transmission spectra were used in the data analysis for both Region I (800–1100 cm^{-1}) and Region II (1340–1524 cm^{-1}), as tabulated in Table 3. The spectra were frequency-calibrated against the water (H_2O) transitions observed in the 1400–1550 cm^{-1} region; these features arise from residual water vapor in the FTS chambers at room temperature, not from the gas cell. Frequency calibration factors were derived for

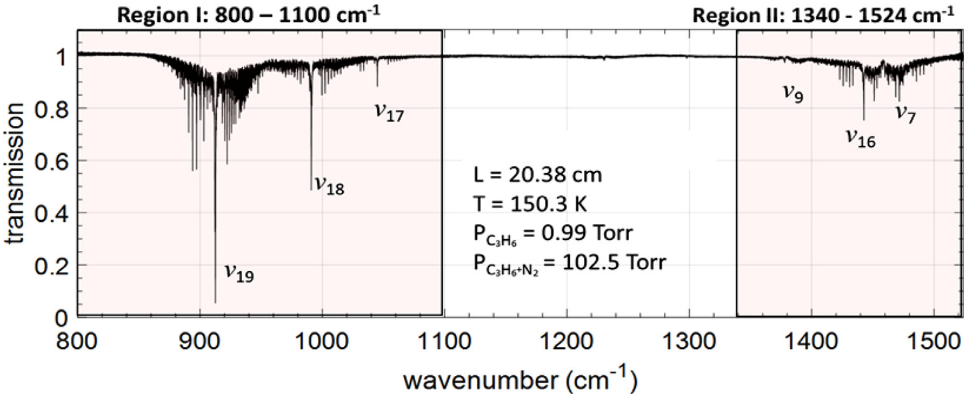

Fig. 2. An example of N_2-pressure broadened spectra of C_3H_6 at 150.3 K, showing two respective spectral regions studied in this work.

all the individual high-resolution spectra (*i.e.* B0117 and B0132 series) by comparing the observed water line positions to those from HITRAN 2012 [48,66]. For B0164 series obtained at high pressures (near 1 Amagat) at low resolution, the calibration factors were obtained from empty-cell spectra at every temperature. Finally, the calibration factors were applied to their corresponding transmittance spectra prior to spectrum analysis, which resulted in a frequency uncertainty better than 5×10^{-4} cm^{-1}.

The monochromatic transmittance $\boldsymbol{\tau}$ at frequency $\boldsymbol{\nu}$ for a series of absorption lines at $\nu_{o,i}$ can be expressed by Eq. (1a). After convolution with the instrumental line shape function (*ILS*) of the FTIR, the observed transmittance τ_{obs} is obtained by Eq. (1b)

$$\tau(\nu) = exp\left\{-\sum S_i \psi_i(\nu - \nu_{o,i}) n \xi l\right\} \tag{1a}$$

$$\tau_{obs}(\nu) = \tau(\nu) * ILS(\nu) \tag{1b}$$

where S_i is line intensity (cm^{-1}/(molecule cm^{-2}) of the *i*th absorption line, $\psi_i(\nu - \nu_{o,i})$ is a unit-area molecular line shape profile at the given temperature and pressure, n is total number density (molecules/cm^3) of the gas mixture with ξ being the mixing ratio of the absorbing gas, and l is absorption path length (cm) of the cell. In a fully-resolved spectrum, with the absorption features wider than ILS(ν), the convolution becomes a do-nothing operation, so we can write

$$\kappa_{obs}(\nu) \ = -\sum S_i \psi_i(\nu - \nu_{o,i}) \tag{2a}$$

$$\kappa_{obs}(\nu) = -ln\left[\tau_{obs}(\nu)\right]/(n\xi l) \tag{2b}$$

So the cross-sections, κ_{obs}, can be computed from spectroscopic line parameters (intensities and line shape parameters) through line-by-line calculations by Eq. (2a). The advantage of the line-by-line calculations is that they can be calculated at any pressure and temperature conditions, not just the measurement conditions specific to the observed spectra from which the cross sections are derived. One should note that, however, Eq. (2a) is not applicable to derive cross-sections until individual spectroscopic line parameters (*e.g.*, line intensities and shapes) have been generated. Moreover, for polyatomic hydrocarbons like propene, it is hard to resolve their rovibrational transitions and measure their individual spectroscopic line parameters. For instance, pressure-broadened line widths become even more difficult to measure because most transitions are likely to be severely blended in the pressure-broadened spectra. On the other hand, the propene cross-section can be also obtained from the observed transmittance spectrum by Eq. (2b). It should be recalled, however, that the cross-section is an implicit function of pressure *P* and temperature *T via* the molecular line shape function, $\psi(\nu - \nu_o)$ as well, whose information is reduced into a transmittance such that the line shape information cannot be recovered unless the absorption features are fully resolved in the observed spectra. Therefore, the measured cross-sections are pressure and temperature specific, leaving the validity of the measured cross-sections limited to the particular experiment conditions. In order to overcome such a limitation, we measured the cross-sections over a wide range of pressures and temperatures covering the atmospheric conditions of interest. Finally, we present an overview of the measured cross-sections at room temperature in the two spectral regions in Fig. 3, in comparison to those from the earlier studies from KAUST [38], PNNL [5], and NIST [51]. As seen in Fig. 3, non-negligible zero offset is apparent in the low-resolution (*i.e.* 2 cm^{-1}) cross-sections from the NIST data, which is a digitized spectrum of an original in hardcopy created in 1964. Since no further information is available, we have not attempted to perform any zero level offset correction on the NIST spectra prior to the comparison to this work.

Table 4
Total partition function of propene at various low temperatures and the values normalized to that at T_0 = 296 K.

T (K)	Q_{total}	$Q(T)/Q(T_0)$	T (K)	Q_{total}	$Q(T)/Q(T_0)$
300	141237.6	1.0412	170	33662.1	0.2481
296	135654.7	1.0000	150	25987.9	0.1916
270	103950.8	0.7663	130	19678.8	0.1451
250	84229.9	0.6209	110	14505.3	0.1069
230	67840.0	0.5001	90	10275.1	0.07574
210	54238.5	0.3998	80	8463.6	0.06239
190	42972.4	0.3168	70	6832.4	0.05037

As illustrated in Fig. 3, Region I (800–1100 cm^{-1}) includes the relatively well isolated $\nu_{19,}$ ν_{18}, and ν_{17} bands centered at 912.56, 990.8, and 1045 cm^{-1}, respectively, and hot band features near 911.9 cm^{-1}, whose peak drops at lower temperatures toward 190 K in the observed cross-sections (see Fig. 4). It should be recalled that a procession of the prominent strong "lines" across the spectral region is actually series of sub-$^{\Delta Ka}Q_J$ branches for the given strong bands.

Details for the cross-sections near the most prominent *Q*-branch of the ν_{19} band near 912 cm^{-1} in the N$_2$-broadened spectra at five different temperatures are presented in Fig. 4. The individual transitions in *Q*-branches and $^{\Delta Ka}Q_J$ sub-branches are seen to be completely blended and appear as broad absorption features, hindering the retrieval of N$_2$-broadened line widths for individual propene transitions. Since these are direct measurement of the absorption features, the cross-sections at a given frequency include all contributions from unidentified hot and combination bands as well as the fundamental cold bands specified in Table 1.

Finally, as a novel approach to be able to compute cross sections and integrated intensities for given spectral regions by using Eq. (2a) when true spectroscopic line parameters are available for C$_3$H$_6$ in this region, we have generated a set of pseudoline parameters by fitting all the observed spectra simultaneously, which will be described in ensuing sections.

4. Partition function

Multispectrum fitting over a broad temperature range requires a partition function. For propene in this work, the total partition function was computed at the measurement temperatures in two steps following the same approach as practiced for propane in Sung et al. [6] and Drouin et al. [67]. Firstly, the vibrational partition function, Q$_{\text{vib,}}$ was computed with the Harmonic Oscillator approximation, which can be expressed by

$$Q_{vib} = \prod_{n=1}^{20}\left[1 - \exp\left(\frac{-C_2 E_n}{kT}\right)\right]^{-d_n} \tag{3}$$

where C_2 = 1.4388 cm^{-1}/K, n is an index of the normal modes (n = 1–20 for propene, excluding the methyl torsion, n = 21). The degeneracy, d_n, is unity for all the modes. Vibrational band centers, E_n, are presented in Table 1. We next computed the sum-over-states $Q_{rot\text{-}tor}$ partition function by considering the ground state, the ν_{21} torsional state and its five torsional excitations using a Hamiltonian model in SPCAT [68], in which the rotational levels were taken into account by up to J_{max} = 99. Finally, the total partition function obtained as the product of the two, Q_{vib} and $Q_{rot\text{-}tor,}$ whose final values at the given temperatures are presented in Table 4.

In order to facilitate the implementation of the partition function into the spectrum fitting algorithm for line-by-line calculations, we fit a second order rational function to the values in the last column of Table 4, (*i.e.* the total vibration-rotation-torsion partition function, Q_{tot}, ratioed to the value at T_0 = 296 K), which can

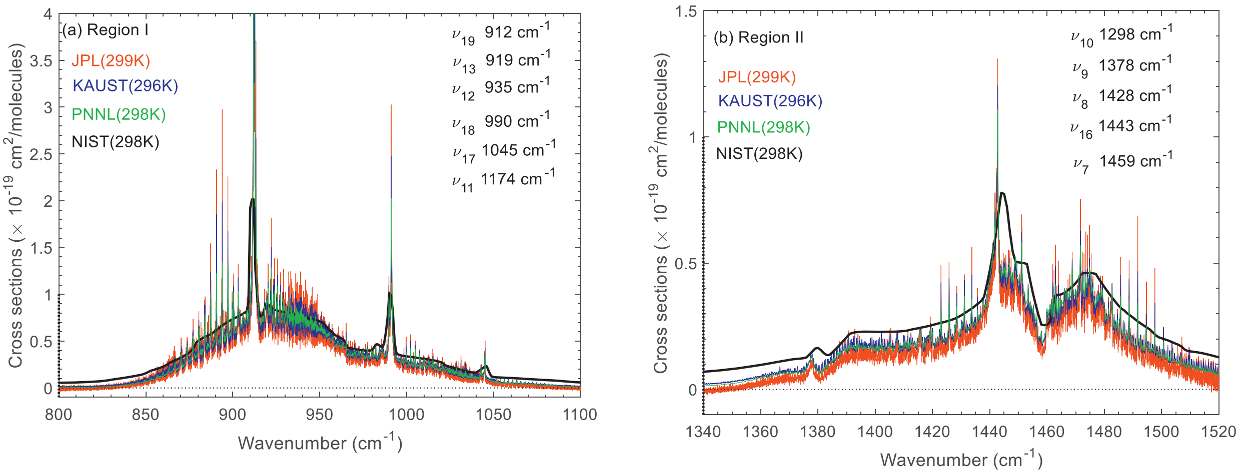

Fig. 3. A sample of cross-sections derived from the transmittances at 4.6 Torr of propene in N_2 having total pressure of 110 Torr; (a) for Region I: 800–1100 cm^{-1} and (b) for Region II: 1340–1524 cm^{-1}, for the present work at 296 K (red curves). These are compared with earlier work: KAUST [38] (blue curves), a normalized composite spectrum from PNNL [5] (green curves), and NIST [NIST Chem Webbook, [51]] (black curves). (For interpretation of the references to color in this figure legend, the reader is referred to the web version of this article.)

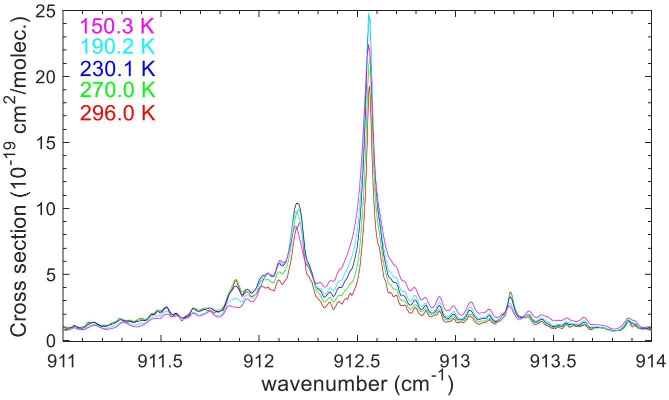

Fig. 4. Cross-sections of N_2-broadened propene in the *Q*-branch region of the ν_{19} band near 912.56 cm^{-1} at five temperatures (150.3, 190.2, 230.1, 270.0, and 296.0 K. Note that there is a hot band feature at 911.87 cm^{-1} that disappears at the two lowest temperatures. Part of the feature at 913.28 cm^{-1} seems to belong to the Q-branch of ν_{18} (CH_2 wagging) band of ^{1}D-propene (CH_3–CD=CH_2) (Silvi et al. [40]).

be readily implemented into an existing spectrum fitting program package, GFIT [69] employed in this work.

$$\frac{Q_{tot}(T)}{Q_{tot}(T_o)} = \frac{a_0 + a_1 T}{b_0 + b_1 T + T^2} \tag{4}$$

with the coefficients being (a_0, a_1) = (−3264, 150.4) and (b_0, b_1) = (2.055 × 10^5, −850.9); this model was used in the spectrum fitting described in the following section. As shown in Fig. 5, the partition function ratios, *i.e.* $Q_{tot}(T)/Q_{tot}(T_o)$ from the SPCAT calculations can be reproduced using this model within ±1% at temperatures down to 100 K.

5. Pseudoline generation

As in the earlier analyses of C_3H_8 and C_6H_6 [6,71], we have generated a HITRAN-format empirical PLL for propene. Such a line list provides a practical way to calculate spectral features of C_3H_6 that accurately reproduce the observed cross-sections at any temperatures and pressures encompassed by the measurements. We briefly summarize the basic assumptions and advantages of the pseudoline generation approach. Firstly, it is assumed that valid average transmission values can be defined for a given frequency grid, typically (but not necessarily) uniformly-spaced wavenumber bins, which are regarded as the ‘pseudoline’ positions. The pseudolines are treated as spectroscopic transitions whose descriptive parameters consist of intensities, lower state energies, and line shape parameters (*e.g.* pressure-broadened widths and frequency shifts, and their temperature dependences) for every individual pseudoline. This approach has been successfully applied to the Earth atmospheric remote sensing [69,70,72]. Then, we derived intensity parameter *S* at 296 K and an effective lower state energy *E*″ for all the individual pseudolines (*i.e.* the frequency bins) in the 800–1100 and 1340–1524 cm^{-1} region by simultaneously fitting the four pure and 23 N_2-broadened propene spectra recorded at 150–299 K (See Table 3). For the pseudoline position parameter, the frequency

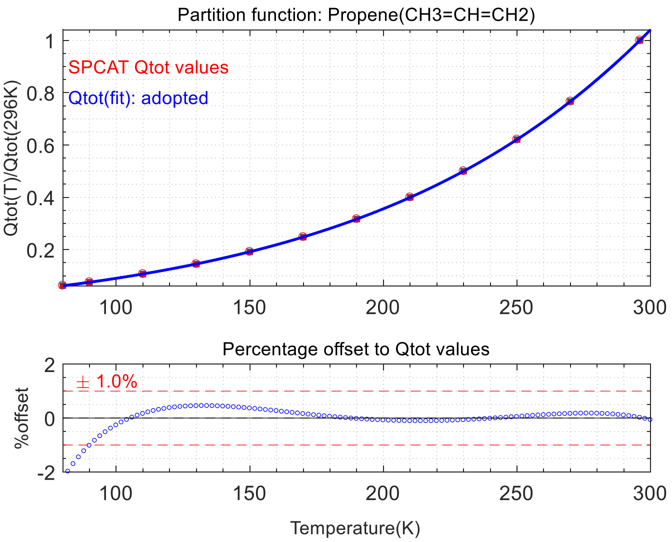

Fig. 5. Total partition function (Q_{tot}) of propene (C_3H_6) normalized to that at 296 K. From 300 K down to 100 K, the model parameters from Eq. (4) (solid blue curve) are within 1% of the corresponding values from the realistic partition function, Q_{tot} from the SPCAT calculations (red symbols) combined with Harmonic Oscillator Approximation. (For interpretation of the references to color in this figure legend, the reader is referred to the web version of this article.)

Table 5
List of all the assumed parameters at 296 K in the pseudoline generation.

Parameters	Values	Ref.
Frequency grid spacing	0.005 cm^{-1}	*See text*
Modified Doppler full width (fixed)	0.005 cm^{-1}	*See text*
γ_{N2} in the 912–913 cm^{-1} region	0.11 cm^{-1}/atm	Assumed based on Devi et al. [60]
γ_{N2} in all other region	0.12 cm^{-1}/atm	
γ_{self} in the 912–913cm^{-1}	0.15–0.17 cm^{-1}/atm	
γ_{self} in all other region	0.18 cm^{-1}/atm	
n, T-dependence for pressure-broadened width	0.7	
Pressure-induced frequency shift	−0.003 cm^{-1}/atm	Assumed; *See text*

Notes: γ_{N2}= N_2-broadened half width; γ_{self} = Self-broadened half width

spacing was chosen to be 0.005 cm^{-1} by trading off the precision of the retrieved pseudoline parameters (intensity and lower state energy) and computation efficiency of the PLL in a line-by-line calculation model. The finer the pseudoline spacing adopted, the better the fits to the lab spectra, but the resulting PLL becomes larger and requires more computation to use it. At some point the improvement in the fits to the lab spectra becomes meaningless (*i.e.*, fitting their noise).

For every individual pseudoline, a Voigt line shape profile was employed, which was convolved with an instrument line shape function (for the FTS being a *sinc* function with field-of-view correction). For the Doppler line broadening, the full width was assumed to be the same as the line spacing, *i.e.*, 0.005 cm^{-1}, and was therefore held fixed for all temperatures. This Doppler width functions as a constant minimal width to simulate continuous or featureless absorption effects contributed by unidentifiable numerous weak features. The same pressure-broadened half-width coefficients and temperature dependences were adopted for all pseudoline transitions (*i.e.*, the frequency bins). It was not possible to derive these coefficients from the measured spectra because the C_3H_6 absorption features are so densely spaced that their individual rovibrational transitions are hardly resolved. It is not surprising that no measurement is available for Lorentz half widths of propene thus far. Therefore, we have assumed 0.12 and 0.18 cm^{-1}/atm at 296 K for N_2-broadened (γ_{N2}) and self-broadened widths (γ_{self}), respectively, along with the temperature dependence exponent n being 0.7 in Eq. (5) for both self- and N_2-broadened half widths. These were adopted from the values observed for another polyatomic hydrocarbon species, C_2H_6 [60]. However, slightly smaller values of width at 296 K, 0.11 cm^{-1}/atm for the N_2-broadened width and 0.15–0.17 for the self-broadened width, were adopted in the 912–913 cm^{-1} region, were found to produce better fitting residuals for the Q-branch features of the ν_{19} band. The N_2-pressure induced frequency shift was assumed to be −0.003 cm^{-1}/atm, also analogous to C_2H_6. All the assumed parameters in the pseudoline generation are summarized in Table 5.

$$\gamma(T) = \gamma(T_o) \times (T_o/T)^n \tag{5}$$

As part of the multispectrum fitting procedure, the line strengths (S) and lower state energies (E'') of the individual pseudolines were adjusted by

$$\frac{S(T)}{S(T_0)} = \frac{Q_{tot}(T)}{Q_{tot}(T_0)} \times \frac{SE(T)}{SE(T_0)} \times e^{C_2E''\left(\frac{1}{T_0}-\frac{1}{T}\right)} \tag{6}$$

where $S(T_o)$ is the line strength in cm^{-1}/(molecule cm^{-2}) at T_o = 296 K. Q_{tot} is the total partition function computed in the earlier section, SE(T) = [1 − exp(−$c_2\nu_i/k$T)] is the correction for the Stimulated Emission, ν_i being the pseudoline position (cm^{-1}). Further details on the spectrum fitting and pseudoline generation process can be obtained from the on-line document (https://mark4sun.jpl.nasa.gov/pseudo.html) and Sung et al. [6,71], which will not be repeated here. It should be noted, however, that spurious H_2O absorption features, which survived in the ratioed spectra due to the water vapor variations in the FTS enclosure from spectrum to spectrum, were also fitted by using the known water line parameters. As a result, the PLL of propene compiled in this work is free of the H_2O line feature contamination. The pseudoline parameters, like true spectroscopic line parameters, are instrument- or resolution-independent, and they can be used with any existing line-by-line calculation model as an effective spectroscopic input.

Finally, PLLs for C_3H_6 are compiled as separate electronic supplements. A small segment of the compiled PLL is presented in Table 6 for the Q-branch region of ν_{19} band near 912.67 cm^{-1}. It should be noted that the molecule index (two digits) has been set to be 74, which is an arbitrary choice that can be changed by the user. The isotopologue index has been set to be zero in order to explicitly indicate these parameters are for pseudolines rather than for true spectroscopic transitions. The fitting residuals are presented in Fig. 6 with the numbers of spectra at each measurement temperature indicated in the plot labels. One can see that the largest fitting residuals are localized near the Q-branch region of each band. Only the results for the N_2-broadened spectra are shown in Fig. 6, which would be representative of observed atmospheric spectra of Titan, in which N_2 is the dominant atmospheric constituent. The synthetic spectra representing the two spectral regions were generated at all the temperatures and pressures of measurements by using one single PLL at 296 K compiled in the HITRAN line list format [48]. Noisier residuals are seen for the pure sample spectra (not presented here for sake of clarity), which are ascribed to a lower S/N that resulted from scanning at a very high spectral resolution (0.0022 cm^{-1}). In the pure C_3H_6 spectrum set at low pressures, observed absorption features retain structures much finer than the spectrum grid, 0.005 cm^{-1}. As seen in Fig. 6, all of the N_2-pressure broadened spectra show fitting residuals better than 2%, except for the ν_{19} Q-branch region showing bigger residuals up to ∼8%, which can be ascribed to line mixing effects, especially for the spectra obtained at high pressures.

We have investigated the validity of the pseudoline generation to assess the derived pseudoline parameters (*i.e.* intensities and lower state energies) by inspecting the distribution of the lower state energies *vs.* the line intensities, as presented in Fig. 7. The lower state energy retrieved from the multispectrum fitting by pseudolines should be regarded as an effective mean value representing multiple spectroscopic transitions falling in that frequency bin (*i.e.* pseudoline position) from many weak and/or hot band features in addition to the fundamental bands. Thus, the retrieved effective lower state energies tend to be higher than the typical values for “true” spectroscopic parameter sets that ignore overlapping hot band features. Such is especially true for polyatomic hydrocarbons bearing low-lying states such as a torsional band. As seen in Fig. 7, the propensity of having higher values for the lower state energies was picked up well by the pseudoline generation.

Table 6
An excerpt of the pseudo-linelist for propene in a column separated format.

MM	I	wn(cm^{-1})	S(296K)	γ(N2)	γ(self)	E″(cm^{-1})	n	shift
74	0	912.600	2.795E-21	0.1100	0.1500	168.5899	0.70	-0.003000
74	0	912.605	3.340E-21	0.1100	0.1500	4463.1362	0.70	-0.003000
74	0	912.610	3.969E-21	0.1100	0.1500	306.3909	0.70	-0.003000
74	0	912.615	8.265E-21	0.1100	0.1500	241.8318	0.70	-0.003000
74	0	912.620	1.040E-21	0.1100	0.1500	5931.9243	0.70	-0.003000
74	0	912.625	3.463E-21	0.1100	0.1500	145.6729	0.70	-0.003000
74	0	912.630	4.074E-21	0.1100	0.1500	507.0706	0.70	-0.003000
74	0	912.635	1.230E-22	0.1100	0.1500	1869.2985	0.70	-0.003000
74	0	912.640	9.839E-23	0.1100	0.1500	6301.0991	0.70	-0.003000
74	0	912.645	6.525E-21	0.1100	0.1500	198.7001	0.70	-0.003000
74	0	912.650	1.324E-21	0.1100	0.1500	973.6246	0.70	-0.003000
74	0	912.655	1.546E-22	0.1100	0.1500	3096.2705	0.70	-0.003000
74	0	912.660	1.223E-21	0.1100	0.1500	4348.9141	0.70	-0.003000
74	0	912.665	2.508E-24	0.1100	0.1500	6137.7412	0.70	-0.003000
74	0	912.670	5.031E-21	0.1100	0.1500	196.0108	0.70	-0.003000
74	0	912.675	1.127E-21	0.1100	0.1500	73.3962	0.70	-0.003000
74	0	912.680	1.531E-21	0.1100	0.1500	640.8004	0.70	-0.003000
74	0	912.685	2.598E-22	0.1100	0.1500	2919.8848	0.70	-0.003000
74	0	912.690	1.174E-21	0.1100	0.1500	1895.7051	0.70	-0.003000
74	0	912.695	3.091E-21	0.1100	0.1500	251.6637	0.70	-0.003000
74	0	912.700	3.069E-22	0.1100	0.1500	1155.1521	0.70	-0.003000
74	0	912.705	5.385E-21	0.1100	0.1500	152.0501	0.70	-0.003000
74	0	912.710	2.708E-25	0.1100	0.1500	5558.9502	0.70	-0.003000
74	0	912.715	4.883E-22	0.1100	0.1500	1339.8115	0.70	-0.003000
74	0	912.720	7.335E-22	0.1100	0.1500	3050.7393	0.70	-0.003000
74	0	912.725	9.581E-22	0.1100	0.1500	221.3239	0.70	-0.003000
74	0	912.730	2.378E-21	0.1100	0.1500	545.5908	0.70	-0.003000
74	0	912.735	3.019E-24	0.1100	0.1500	3259.3555	0.70	-0.003000
74	0	912.740	4.089E-24	0.1100	0.1500	1053.4281	0.70	-0.003000
74	0	912.745	4.938E-21	0.1100	0.1500	148.0366	0.70	-0.003000
74	0	912.750	6.380E-24	0.1100	0.1500	4784.8311	0.70	-0.003000
74	0	912.755	1.526E-22	0.1100	0.1500	4474.3066	0.70	-0.003000
74	0	912.760	8.191E-22	0.1100	0.1500	422.8178	0.70	-0.003000
74	0	912.765	1.403E-21	0.1100	0.1500	445.9078	0.70	-0.003000
74	0	912.770	1.635E-22	0.1100	0.1500	9.3277	0.70	-0.003000
74	0	912.775	9.700E-22	0.1100	0.1500	1688.0457	0.70	-0.003000
74	0	912.780	2.836E-22	0.1100	0.1500	917.8647	0.70	-0.003000
74	0	912.785	2.634E-28	0.1100	0.1500	3630.3979	0.70	-0.003000
74	0	912.790	3.679E-21	0.1100	0.1500	118.6220	0.70	-0.003000
74	0	912.795	2.352E-24	0.1100	0.1500	0.0000	0.70	-0.003000
74	0	912.800	2.201E-21	0.1100	0.1500	287.1741	0.70	-0.003000

Notes: MM = molecule index; I = isotopologue index. Set I = 0 as an indicator of pseudoline entry; wn = wavenumber in cm^{-1}; S = line intensity of propene in natural abundance at 296K in cm^{-1}/(molecule.cm^{-2}); γ = half width for N_2-broadening and for Self-broadening in cm^{-1}/atm; E'' = lower state energy (cm^{-1}); n = temperature dependence exponent for pressure broadened widths; Pressure-induced frequency shifts (cm^{-1} /atm). Note that the full list can be found in the electronic supplement in the HITRAN format. For further details on the HITRAN data format, See the HITRAN database [48–50].

An elongated tail toward higher values for the lower state energy is noticeable in Fig. 7 for both Region I and Region II. The derived lower state energy values exceeding ~2000 cm^{-1} are needed to reproduce the continuum-like absorption features that result from so many hot and weak band features overlapped in the respective spectral bin.

The retrieved pseudolines were also examined for any possible systematic bias in the retrieval of the input sample conditions, in particular, the sample pressures. Recalling that the fitting residuals presented here are obtained from multispectrum fitting using one pseudo line list (PLL), and that all the 27 spectra were recorded at various pressures and temperatures, any deviation in the spectrum-to-spectrum consistency could be regarded as measurement uncertainty for the PLL. In order to inspect such a possible bias, we have adopted the PLL as spectroscopic input in a radiative transfer model and retrieved volume mixing ratio (VMR) scale factors for the individual laboratory spectra. Ideally, the retrieved VMR scale factors would all be unity, meaning that the known sample pressure readings listed in Table 3 would have been reproduced perfectly.

As presented in Fig. 8, the retrieved VMR scale factors ranged from 0.92 to 1.14 in Region I and 0.91 to 1.14 in Region II, whose overall mean values were 1.008 (±0.053) and 1.008 (±0.070), respectively. In other words, the mean retrieved VMR scale factors are only 0.8% away from the ideal values for both regions with their standard deviations being 5.3% and 7.0%, respectively. The large standard deviations can be taken as the actual overall measurement uncertainties associated with the PLL determined in this work. Such an uncertainty level looks very reasonable, considering the intrinsic limitations brought by the several assumptions made for the pseudoline generation (*e.g.*, one value of the mean lower state energy for a given frequency bin which can contain multiple transitions of different lower state energies, a constant value of pressure-broadening for all the pseudolines, the assumed temperature dependence defined by Eq. (5), etc.). Besides, there are several other factors contributing to the retrieval error, which includes spectral noise, disturbance of the 100% transmission level, interfering molecules (*i.e.*, residual H_2O), and volume mixing ratio uncertainty introduced by the mixture preparation. All of these contribute to the overall measurement uncertainties.

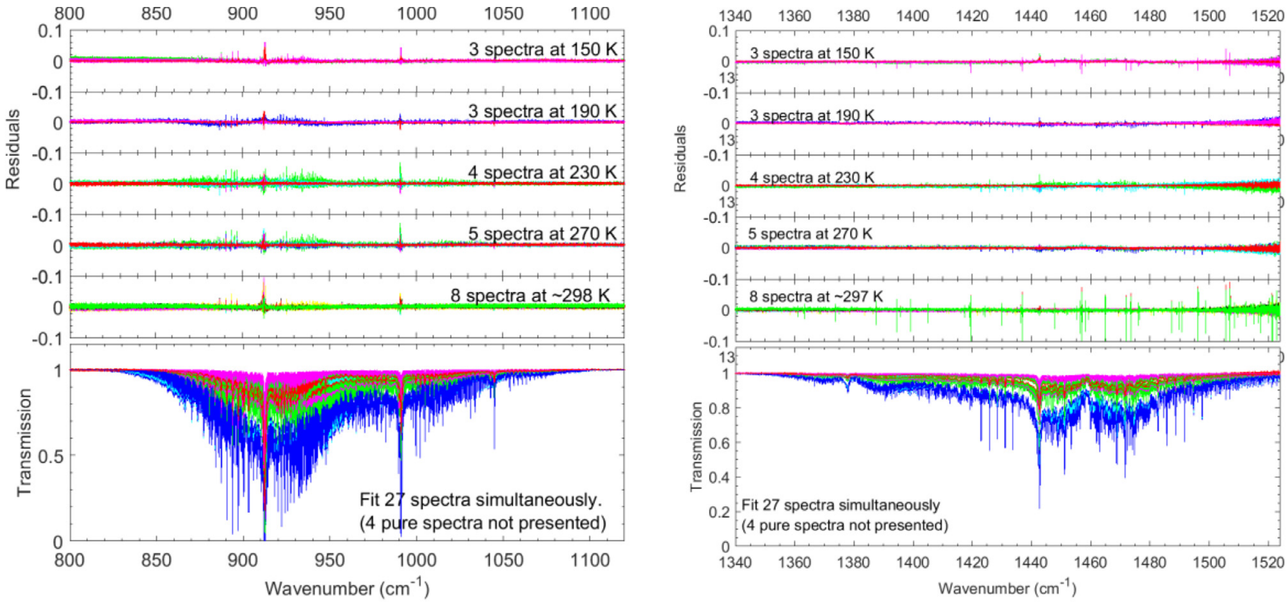

(a) (b)

Fig. 6. [Top panel] Each panel (ranging ±0.1, *i.e.* 10%) shows that fitting residuals from the C_3H_6+ N_2 mixture spectra for (a) Region I (Left) and (b) Region II (Right) are within 5% for the individual experiment conditions, and [Bottom panel] all the synthetic spectra based on one single PLLt.

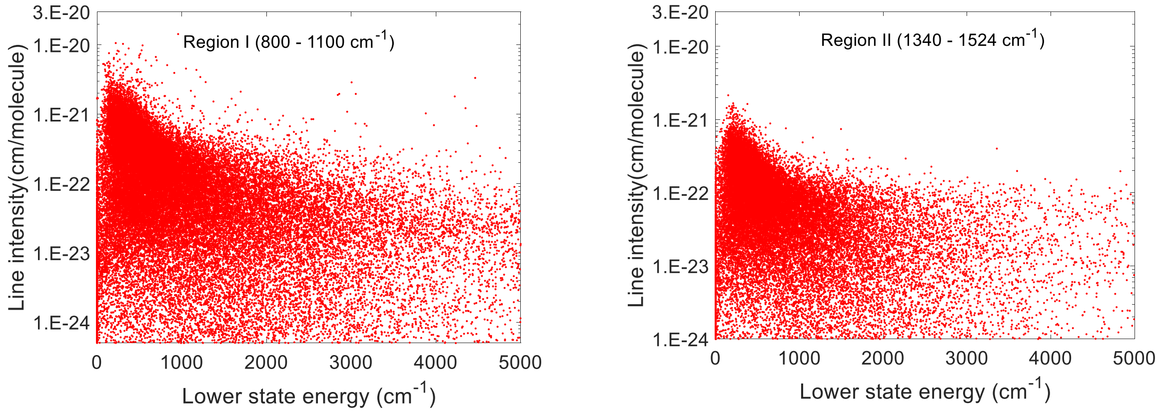

Fig. 7. Distribution of the effective lower state energies *vs.* the line intensities from the PLL determined in this work.

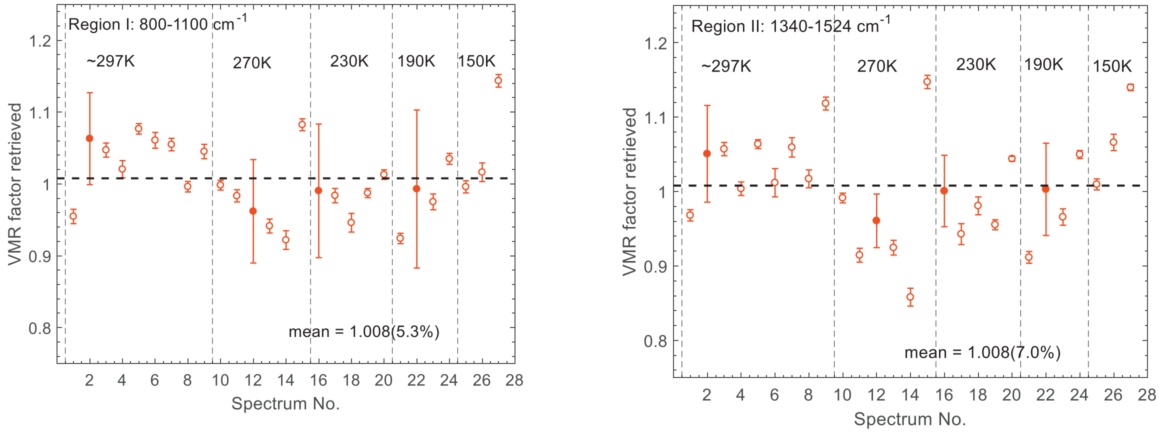

Fig. 8. Retrieved volume mixing ratio (VMR) scale factors for the respective individual laboratory spectra of pure C_3H_6 sample (solid circle) and of mixtures with N_2 (open circle). Left panel shows Region I. Right panel shows Region II. Mean value of the VMR scale factor was observed to be 1.008 for both Regions with standard deviation being 5.3% for Region I and 7.0% for Region II, which could be considered as overall measurement uncertainties for the C_3H_6 pseudoline list.

Table 7
Integrated intensity, A_B in 10^{-18} cm^{-1}/(molecule cm^{-2}) of the C_3H_6 (100% purity normal sample) in the region specified at various cold temperatures.

Sources	Region I 800–1100 (in cm^{-1}) ν_{19}, ν_{18}, ν_{17}	Region II 1340–1524 (in cm^{-1}) ν_9, ν_{16}, ν_7
JPL (298 K)	8.79(47)	3.06(21)
JPL (296 K)	8.79(47)	3.06(21)
JPL (278 K)	8.87(47)	3.13(22)
JPL (270 K)	8.93(47)	3.17(22)
JPL (230 K)	9.21(49)	3.35(23)
JPL (190 K)	9.10(48)	3.41(24)
JPL (150 K)	8.29(44)	3.18(22)

Notes: The uncertainties are given in the unit of the last quoted digit.

6. Results and comparison

6.1. Integrated intensities over bands

We note that band intensity, S_v cm^{-1}/(molecule cm^{-2}), is considered as one of the most useful spectroscopic properties of a molecule, providing insight on molecular structure and band-to-band interactions as well as a practical guideline for applications in atmospheric remote sensing. An integrated intensity over a given spectral range bearing a band (or bands) well isolated from neighboring features, $\boldsymbol{A_B}$ in cm^{-1}/(molecule cm^{-2}), can be obtained by summing up all line intensities over the spectral region and also can be written using the band intensity, S_v:

$$A_B(T) \approx S_v \times Q_{vib}(T) \tag{7}$$

where Q_{vib} is vibrational partition function at a given temperature *T*. For isolated fundamental bands, their band intensity is known to be independent of temperature [73,74]. Meanwhile, an integrated cross section, $\boldsymbol{X_B}$ in cm^{-1}/(molecule cm^{-2}) over the spectral bins, is computed by summing up the measured cross-sections over the range of wavenumbers for a given band or bands. However, as discussed in Sung et al. [6], the integrated cross section, $\boldsymbol{X_B}$, for particular band(s) spanning a spectral range is not necessarily equal to the integrated intensity, A_B, over the same spectral range. Some strong features in the observed spectrum could fall out of the linear relationship between the equivalent width and the number density of the absorbing gas. These are particularly expected for heavy molecules with strong Q-branch features. In the mid-infrared region, Doppler widths are very small, beyond the instrumental resolutions available for a conventional broad-band FT-IR. As we see in Fig. 2, propene has prominent Q-branches, and that of the ν_{19} band near 912.67 cm^{-1} reached near saturation in our observed spectra. Therefore, instead of integrated cross section, $\boldsymbol{X_B}$, we have estimated integrated intensity, $\boldsymbol{A_B}$, by summing up individual pseudoline intensities in the respective spectral Regions I and II. Compared to the values obtained by other band models or by summation of measured cross-sections, the PLL derived by adopting the Voigt line shape profile in this work would provide an even more physically sound line intensity sum so that the integrated intensity can be more accurate for blended/overlapping bands to be treated all together.

6.2. The integrated intensities and comparison

Based on the pseudoline intensities determined from this work, we could compute the integrated intensities at any temperatures between 299–150 K covered by these laboratory measurements, including 298, 296 and 278 K for direct comparison to earlier work on propene. Our values of the integrated intensities estimated at various temperatures from 298 to 150 K in the designated spectral ranges are presented in Table 7 and in Fig. 9.

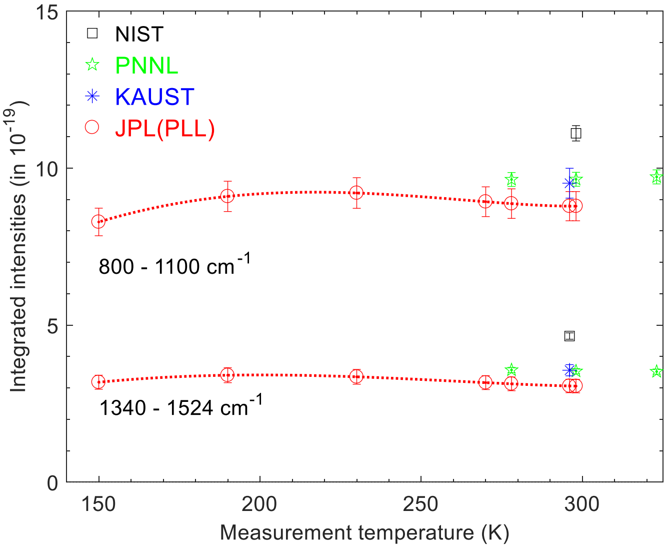

Fig. 9. Our integrated intensities (cm^{-1}/(molecule cm^{-2})), labeled as JPL(PLL), at various temperatures are compared to those from KAUST [38], PNNL [5], and NIST [51]. Temperature dependence of the measured integrated intensities at 278 K, 298 K, and 323 K is compared for the two Regions between the results from this work (red symbols) and PNNL (Sharpe et al. [5]) (green symbols). (For interpretation of the references to color in this figure legend, the reader is referred to the web version of this article.)

One of the advantages with the pseudoline generation approach is that the empirical lower state energies are provided for all the individual pseudolines (*i.e.* transitions). One can convert the pseudoline intensities given at 296 K to other temperatures within our measurement temperature range (296–150 K), from which the integrated intensities over a given frequency range at any cold temperature down to 150 K may be obtained by summing the pseudoline intensities at that temperature. In Fig. 9, the integrated intensities, $\boldsymbol{A_B}$, estimated from the present work at cold temperatures are presented, in which a slight temperature dependence of the integrated intensities can be seen in the 296–150 K range, with the values peaked in the 230–190 K range for both regions. Similar temperature dependences have been observed for the C_3H_8 and C_6H_6 integrated intensities estimated by the pseudoline generation approach [6,71].

The integrated intensities for Region I and II are compared with the early work from direct cross section measurements: KAUST [38], PNNL [5], and NIST [51]. We recall that significant zero level offsets in the NIST data set are apparent, as seen in the cross section spectra shown in Fig. 3. However, it was not straightforward to determine the true zero level from their cross section spectra since no further information can be found in the NIST data set. Keeping this minor subtlety in mind, we made a direct comparison of the integrated intensity without any zero-offset correction. However, it should be noted that KAUST [38] made comparison of their integrated intensities with those from earlier works after a zero-offset correction on all the comparison data sets (including those of PNNL). Thus, we made an additional comparison with their original data set in the electronic supplement of the cited publication [38]. The comparison at 298, 296, and 278 K with the relevant sets of earlier work in the designated spectral ranges are presented in Table 8 and in Fig. 9.

For Region I (800–1100 cm^{-1}), where the ν_{19} band is the primary opacity source, we note that our measurements are significantly lower than the KAUST [38] with no baseline correction and the PNNL values [5] at both temperatures (*i.e.* 296 and 278 K) by nearly 8–10%. This discrepancy is beyond the combined measure-

Table 8
Comparison of the integrated line intensity, A_B in 10^{-18} cm^{-1}/(molecule cm^{-2}) at 298 and 278 K of previous published studies, whose values and percentage differences are presented with respect to the this work. The uncertainties in A_B are given in parentheses in the units of the last quoted digit.

Sources[a]		Region I 800–1100 (in cm^{-1})		Region II 1340–1524 (in cm^{-1})	
		A_B	%Δ[b]	A_B	%Δ[b]
At T = 298K	Res. (cm^{-1})[c]				
JPL (This Work)	0.0022–0.042	8.79(47)		3.06(21)	–
KAUST(Table 3)[d]	0.05	8.75(20)	−0.4%	2.90(10)	−5.1%
KAUST(spectrum)[e]	0.05	9.52(48)	8.3%	3.56(10)	16.4%
PNNL	0.062	9.65(21)	9.7%	3.53(8)	15.1%
NIST	2.0	11.11	26.4%	4.65	52%
At T=278K					
JPL (This work)		8.87(47)		3.13(2)	–
PNNL	0.062	9.64(21)	8.7%	3.57(8)	14.1%

[a] KAUST [38], PNNL [5], and NIST [51].

[b] %Δ(wrt JPL) = (Other–JPL)/JPL*100 at the given temperature.

[c] Spectral resolution, defined by 0.5/MOPD, where MOPD is Max. Optical Path Difference.

[d] Their reported values are adjusted for comparison over the common spectral ranges based on their spectrum.

[e] Based on their spectrum reported as an electronic supplement with no baseline correction.

ment uncertainty of 7.3% for KAUST and 5.8% for PNNL. It is not clear to us what caused this discrepancy. However, it is interesting to note that, in case of the C_3H_6 cross-sections in the 3 µm region (2500–3200 cm^{-1}), the integrated intensity value at room temperature reported by Buzan et al. [57] based on spectra obtained at the highest resolution (up to 0.005 cm^{-1}) is also lower than the PNNL value by 3.4% prior to normalizing their cross-sections to the mean value of the PNNL data. The values of NIST, whose spectral resolution were the lowest among the comparison sets, shows even greater differences than those of KAUST and PNNL, but no information on their measurement uncertainties is found, so that a proper quantitative evaluation cannot be made. Initially, Es-sebbars et al. [38] reported 8.62(20) and 3.01(10)× 10^{-18}cm^{-1}/(molecule cm^{-2}) in the 800–1060 cm^{-1} and 1340–1550 cm^{-1} region, respectively, after a baseline correction. To facilitate a direct comparison, their values are adjusted to the common spectral ranges of the Region I and II based on their own spectrum. Interestingly, their reported integrated intensity for Region I is slightly lower than our measurement~~s~~ by 0.4%. For Region II (1340–1524 cm^{-1}), the integrated intensity from this work at room temperature (296 K) is measured to be substantially lower than the KAUST [38] and the PNNL [5] values. The NIST [51] value shows a significant discrepancy by more than 50%, as was noticed by Es-sebbars et al. [38] even after the zero-offset correction on the NIST data set by Es-sebbars et al. Our measurement at 278 K in Region II is also significantly lower than the PNNL value by 14.1%, which is outside the combined measurement uncertainties, 7.3% with KAUST and 5.3% with PNNL.

6.3. Error estimates and isotopologues contribution

We have estimated error budgets considering the uncertainties associated with the experimental inputs such as temperature drift, path length of the gas cell, pressure reading, zero-offset, 100% transmission level drifts due to ice absorption features, and uncertainty in the mixing ratio. Among them the last two are the biggest contributors to the error budget. Firstly any offset from the 100% transmission level caused by ice absorption, which grows during the period that the cell is kept cold, was determined to be less than 0.5% by selectively taking empty-cell spectra as a consistency check. Well-localized weak absorption features, which could be attributed to water ice, appear in the 1068.4–1075.5 and 1258.2–1299.3, and 1447.4–1472.5 cm^{-1} regions, which were effectively canceled out in the transmittance generation. The spectrum fitting uncertainty associated with the pseudoline intensity was estimated to be less than 1% in both spectral Regions I and II. At the same time, we note that the standard deviations of the retrieved VMR scale factors, 5.3% and 7.0% in Regions I and II, respectively, could be taken as overall measurement uncertainties in the C_3H_6 pseudolines. The overall uncertainties should cover all the uncertainty sources discussed above (*e.g.,* partial pressure in the mixtures, baseline uncertainties, weak ice absorption features, etc.), because the standard deviations of the retrieved VMR scaling factors are a resultant effect after all the factors are taken into account during the multi-spectrum fitting and pseudoline retrievals.

As stated earlier, we used an anhydrous high-purity (>99%) normal sample of propene with no isotope enrichment. Therefore, the propene pseudolines and cross-sections reported in this work do not discriminate or exclude contributions from its two most abundant minor isotopologues; based on the PDB values for $^{13}C/^{12}C$ and D/H, the relative abundances in percent can be computed to be $^{12}C_3H_6$ = 96.65%, $^{13}CC_2H_6$ = 3.24%, $^{12}C_3H_5D$ = 0.07%. Therefore, the integrated intensities accounted for the primary isotopologue of propene, $^{12}C_3H_6$, can be obtained by multiplying the reported integrated intensities in Table 7 by a scale factor of the $^{12}C_3H_6$ isotopologue abundance, 0.9665.

6.4. Discussion on the PLL performance

As a separate and independent performance test of the derived propene pseudolines, we have measured one additional transmission spectrum exactly at the same pressure, temperature, and spectral resolution as the PNNL spectrum (*i.e.* 3.91 Torr of propene sample in the N_2-bath having total pressure of 765 Torr at 297.5 K at spectral resolution of R = 0.112 cm^{-1}, as defined by 0.9/MOPD in their work). The observed spectrum, which was not included in the multispectrum fitting for the pseudoline generation, was compared to synthetic spectra computed based on (1) JPL-PLL, (2) intensity-adjusted JPL-PLL by 5% based on the mean VMR scale factor (VSF) value (presented in Fig. 8) and the claimed measurement uncertainty, (3) a synthetic spectrum at the same conditions as above but calculated using the PNNL cross sections. The results are presented in Fig. 10a. The JPL-Obs and the PNNL spectrum are over-

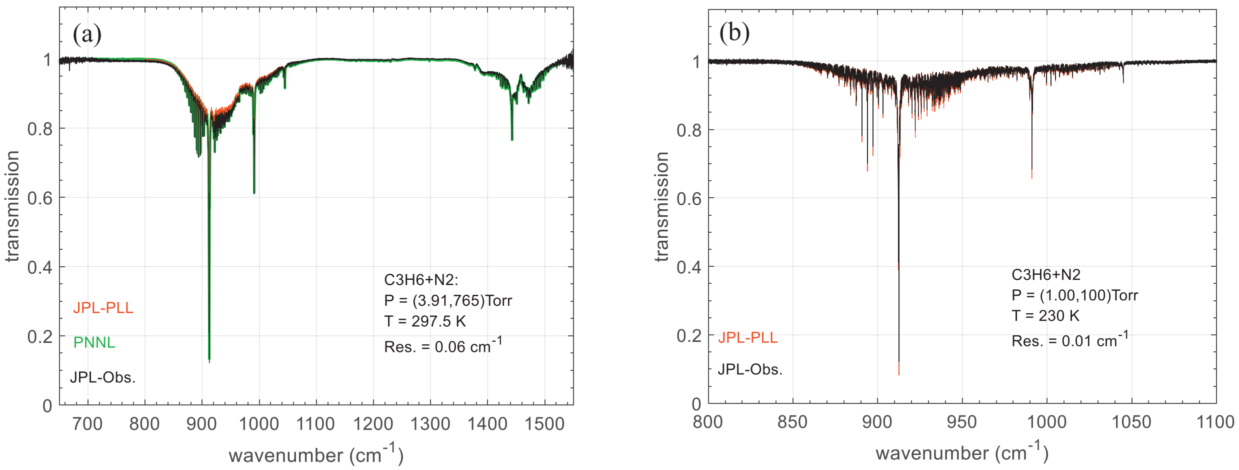

Fig. 10. Comparison of synthetic spectra generated with the JPL-PLL (red) and the PNNL cross-sections (green) with observed spectra (black) at (a) 298 K and (b) 230 K. The PNNL spectrum shows a better agreement with the observed spectrum than the JPL-PLL for the high pressure spectrum at room temperature, while the JPL-PLL reproduces very well an observed spectrum at low pressure (100 Torr) at 230 K . (For interpretation of the references to color in this figure legend, the reader is referred to the web version of this article.)

lapped across the Region I, showing a very good consistency. However, the JPL-PLL underestimates the observed absorption at high pressure (∼ 1 atm) and low resolution (0.06 cm^{-1}). In fact, we already saw this bias at room temperatures in the retrieved VSF values for the spectrum presented in Fig. 8. Seven out of the nine spectra at room temperature have their VSF values greater than unity (up to 1.077), implying that more sample would be needed to reproduce the observed features based on the retrieved PLL. In other words, the PLL intensities are underestimated by the scaling factor when compared to a particular spectrum. As discussed in Section 5, it should be reminded that the pseudoline generation is an approximation, whose intensity and lower state energy values are retrieved with all other parameters being assumed and held fixed (as listed in Table 5), for example, the same pressure-broadened line widths for all transitions with no transition dependence, which is not true.

It is encouraging, however, that a spectrum, B0132.4d, obtained at a much lower pressure (100 Torr) and cold temperature (230 K) with a higher resolution (0.01 cm^{-1}) compared to the one at ∼ 1 atm can be reproduced by the pseudolines. As seen in Fig. 10b, the synthetic spectrum based on the JPL-PLL compiled at 296 K (the one as listed in Table 6) shows an excellent consistency with the observed spectrum. Thus, further laboratory measurements would be needed to determine the pressure-broadened widths and their temperature dependence as well as to produce a true spectroscopic line list through quantum mechanics based modeling study of the C_3H_6 spectroscopy. Until then, this PLL can provide reasonable spectroscopic information in the interpretation of observed spectroscopic features arising from low pressure and cold environment, such as the Titan stratosphere.

7. Conclusions

In support of the atmospheric infrared remote sensing of Titan from ground-based and space-based observations, such as IRTF/TEXES [42] and Cassini/CIRS [1] and upcoming JWST/MIRI [45], we measured absorption cross-sections of C_3H_6 in the 800–1524 cm^{-1} region from 27 pure and N_2-broadened spectra of propene recorded at temperatures from 150 K to 299 K. Accurate interpretation of the CIRS spectra will benefit the understanding of the formation of haze in Titan's cold atmosphere, where large hydrocarbon species formed by photochemical reactions of species such as C_2H with the alkenes, *i.e.*, ethene and propene, and the subsequent reactions of vinylacetylene with C_2H are thought to be primary pathways to the Titan's atmospheric haze [27]. Through simultaneous multispectrum fitting, we also retrieved pseudoline parameters on a 0.005 cm^{-1} frequency grid in two separate spectral regions, Region I (800–1100 cm^{-1}) and Region II (1340–1524 cm^{-1}), which are well isolated from the neighboring absorption features and provide a well-defined 100% transmission level on their spectra boundaries. The PLL includes line strengths and lower state energies as well as other prescribed parameters (positions, self- and N_2-pressure broadened line widths and their temperature dependences, and N_2-pressure induced frequency shifts) for all the individual pseudolines. It was observed that the pseudoline set could reproduce the observed N_2-broadened propene spectrum within 5% at any of the temperature and pressure conditions studied in this work. The combined intensity in both regions, *i.e.* 800–1100 and 1340–1524 cm^{-1}, is estimated to be $11.85(68)\times10^{-18}$cm^{-1}/(molecule cm^{-2}) at 296 K based on the pseudo line list (PLL). Our results estimated at room temperature from the pseudolines are significantly lower than the two recent measurements by PNNL [5] and KAUST [38]. Interestingly, it is observed that the performance of the JPL-PLL is better for reproducing spectra obtained at low pressures and cold temperature, which is indeed encouraging because the PLL approach in this work is designed to provide effective spectroscopic information over the broader temperature range down to 150 K at a wide range of atmospheric pressure conditions.

Several other advantages are also expected when the pseudoline approach is adopted. For heavy polyatomic molecules, such as propene, benzene, and methanol, the contributions from their numerous weak transitions spread across in the mid-infrared region from either hot bands or torsion-related bands are expected to be substantial, affecting the baseline of the atmospheric spectrum. However, they are not easily tractable in quantum mechanical modeling. Therefore, the laboratory spectroscopic constraints inherent in the PLL of propene, which capture all the resultant contribution from the weak transitions, would provide a better chance of revealing new molecular features hidden in the residuals of the Cassini/CIRS spectra.

Finally, the pseudoline list of propene has been compiled in the HITRAN format [48] so that it may be treated as a spectroscopic line parameter list in line-by-line radiative transfer calculations. The pseudoline approach, however, should be regarded as a practical interim solution to provide spectroscopic input in radiative transfer modeling and will be superseded by quantum-mechanically-based spectroscopic line parameters should they become available. Besides, the PLL is a mathematical construct, so that the line list would work best when adopted as a whole for a finite spectral region rather than as independent lines. The cold cross-sections will be submitted to the HITRAN database (http://www.hitran.org/), and the list of C_3H_6 pseudolines will be available from the MK-IV website of JPL (https://mark4sun.jpl.nasa.gov/pseudo.html). The compiled pseudoline lists for Regions I and II have been attached as electronic supplements to this article.

Acknowledgements

Research described in this article was performed at the Jet Propulsion Laboratory, California Institute of Technology, Connecticut College, and NASA Langley Research Center, under contracts and cooperative agreements with the National Aeronautics and Space Administration. K. Sung appreciates insightful discussion and comments from Conor A. Nixon (NASA-GSFC).

Supplementary materials

Supplementary material associated with this article can be found, in the online version, at doi:10.1016/j.jqsrt.2018.03.011.

References

[1] Nixon CA, Jennings DE, Bézard B, Vinatier S, Teanby NA, Sung K, Ansty TM, et al. Detection of propene in Titan's stratosphere. Astrophys J Lett 2013;776:L14.

[2] Hanel R, Conrath B, Flasar FM, Kunde VG, Maguire W, Pearl J, et al. Infrared observations of the Saturnian system from Voyager-1. Science 1981;212:192–200.

[3] Maguire WC, Hanel RA, Jennings DE, Kunde VG, Samuelson RE. C_3H_8 and C_3H_4 in Titan's atmosphere. Nature 1981;292:683–6.

[4] Nixon CA, Jennings DE, Flaud J-M, Bezard B, Teanby NA, Irwin PGJ, Ansty TM, Coustenis A, Vinatier S, Flasar FM. Titan's prolific propane: the Cassini CIRS perspective. Planet Space Sci 2009;57:1573–85. http://dx.doi.org/10.1016/j.pss.2009.06.021.

[5] Sharpe S, Johnson T, Sams R, Chu P, Rhoderick G, Johnson P. Gas-phase data bases for quantitative infrared spectroscopy. Appl Spectrosc 2004;58:1452–61. https://secure2.pnl.gov/nsd/nsd.nsf/Welcome.

[6] Sung K, Toon GC, Mantz AW, Smith MAH. FT-IR measurements of cold C_3H_8 cross-sections at 7–15 µm for Titan atmosphere. Icarus 2013;226:1499–513.

[7] Koyama T, Hayashi Y, et al. Key role of the pore volume of zeolite for selective production of propylene from olefins. Phys Chem Chem Phys 2010;12:2541–54.

[8] Kaiser EW, Siegl WO, Henig YI, Anderson RW, Trinker FH. Effect of fuel structure on emissions from a spark-ignited engine. Environ Sci Technol 1991;25:2005–12.

[9] Baba T, Sawada H. Conversion of methane into higher hydrocarbons in the presence of ethylene over H-ZSM-5 loaded with silver cations. Phys Chem Chem Phys 2002;4:3919–23.

[10] Demaison J, Rudolph HD. Ab initio anharmonic force field and equilibrium structure of propene. J Mol Spectrosc 2008;248:66–76.

[11] Blake DR, Smith TW, Chen T-Y, Whipple WJ, Rowland FS. Effects of biomass burning on summertime nonmethane hydrocarbon concentrations in the Canadian wetlands. J Geophys Res 1994;99:1699 doi:101029/93JD02598.

[12] Yokelson RJ, Susott R, Ward ED, Reardon J, Griffith DT. Emissions from smoldering combustion of biomass measured by open-path Fourier transform infrared spectroscopy. J Geophys Res 1997;102:18865–77.

[13] Burling IR, Yokelson RJ, Akagi SK, Urbanski SP, Wold CE, Griffith DWT, Johnson TJ, Reardon J, Weise DR. Airborne and ground-based measurements of the trace gases and particles emitted by prescribed fires in the United States. Atmos Chem Phys 2011;11:12197–216.

[14] Marcelino N, Cernicharo J, Agundez M, Roueff E, Gerin M, Martin-Pintado J, Mauersberger R, Thum C. Discovery of interstellar propylene (CH_2CHCH_3): missing links in interstellar gas-phase chemistry. Astrophys J 2007;665:L127–30.

[15] Lin Z, Talbi D, Roueff E, Herbst E, Wehres N, Cole CA. Can interstellar propene (CH_3CHCH_2) be formed via gas-phase reactions? Astrophys J 2013;765:80 doi:101088/0004-637X/765/2/80.

[16] Herbst E, van Dishoek EF. Complex organic interstellar molecules. Annu Rev Astron Astrophys 2009;47:427–80.

[17] Herbst E, Roueff E, Talbi D. Radiative association and the formation of interstellar propylene. Mol Phys 2010;108:2171–7.

[18] Pearson JC, Sastry KVLN, Berbst E, de Lucia FC. The Millimeter-Wave and Submillimeter-Wave Spectrum of Propylene (CH_3CHCH_2). J Mol Spectrosc 1994;166:120–9.

[19] Hinkle KW, Keady JJ, Bernath PF. Detection of C_3 in the circumstellar shell of IRC+10216. Science 1988;241:1319–22.

[20] Gottlieb CA, Vrtilek JM, Gottlieb EW, Thaddeus P, Hjalmarson A. Laboratory detection of the C_3H radical. Astrophys J 1985;294:L55–8.

[21] Yamamoto S, Saito S, Ohishi M, Suzuki H, Ishikawa S, Kaifu N, Murakami A. Laboratory and astronomical detection of the cyclic C_3H radical. Astrophy J 1987;322:L55–8.

[22] Thaddeus P, Vrtilek JM, Gottlieb CA. Laboratory and astronomical identification of cyclopropenylidene, C_3H_2. Astrophys J 1985;299:L63–6.

[23] Cernicharo J, Gottlieb CA, Guelin M, Killian TC, Paubert G, Thaddeus P, Vrtilek JM. Astronomical detection of H_2CCC. Astrophys J 1991;368:L39–41.

[24] Snyder LE, Buhl D. Interstellar methylacetylene and isocyanic acid. Nature Phys Sci 1973;243:45–6.

[25] Waite JH Jr, Niemann H, Yelle RV, Kasprzak WT, et al. Ion neutral mass spectrometer results from the first flyby of titan. Science 2005;308:5724.

[26] Cui J, Yelle RV, Vuitton V, Waite Jr JH, Kasprzak WT, Gell DA, Niemann HB, Müller-Wodarg ICF, Borggren N, Fletcher GG, Patrick EL, Raaen E, Magee BA. Analysis of Titan's neutral upper atmosphere from Cassini ion neutral mass spectrometer measurements. Icarus 2009;200:581–615.

[27] Bouwman J, Goulay F, Leone SR, Wilson KR. Bimolecular rate constant and product branching ratio measurements for the reaction of C_2H with ethene and propene at 79 K. J Phys Chem A 2012;116:3907–17.

[28] Hébrard E, Dobrijevic M, Loison JC, Bergeat A, Hickson KM, Caralp F. Photochemistry of C_3H_p hydrocarbons in Titan's stratospheres revisited. Astron Astrophys 2013;552:A132 101051/0004-6361/201220686.

[29] Li C,, Zhang X, Gao P, Yung Y. Vertical distribution of C_3-hydrocarbons in the stratosphere of Titan. Astrophys J Lett 2015;803:L19.

[30] Wilson EH, Atreya SK. Current state of modeling the photochemistry of Titan's mutually dependent atmosphere and ionosphere. J Geophys Res 2004;109:E06002. http://dx.doi.org/10.1029/2003JE002181.

[31] Lavas P, Coustenis A, Vardavas I. Coupling photochemistry with haze formation in Titan's atmosphere, Part I: model description. Planet Space Sci 2008;56:27–66.

[32] Lavas P, Coustenis A, Vardavas I. Coupling photochemistry with haze formation in Titan's atmosphere, Part II: results and validation with Cassini/Huygens data. Planet Space Sci 2008;56:67–99.

[33] Krasnopolsky VA. A photochemical model of Titan's atmosphere and ionosphere. Icarus 2009;201:226–56.

[34] Krasnopolsky VA. Chemical composition of Titan's atmosphere and ionosphere: observations and the photochemical model. Icarus 2014;236:83–91.

[35] Moses JI, Visscher C, Fortney JJ, Showman AP, Lewis NK, Griffith CA, Klippenstein SJ, Shabram M, Friedson AJ, Marley MS, Freedman RS. Disequilibrium carbon, oxygen, and nitrogen chemistry in the atmospheres of HD 189733b and HD 209458b. Astrophys J 2011;737:1–32.

[36] Lafferty WJ, Flaud JM, Herman M. Resolved torsional splitting in the ν_{18} and ν_{19} bands of propene. J Mol Struct 2006;65–69:780–1.

[37] Lide DR Jr, Mann DE. Microwave spectra of molecules exhibiting internal rotation, Propylene. J Chem Phys 1957;27:868–73.

[38] Es-sebbar E, Alrefae M, Farooq A. Infrared cross-sections and integrated band intensities of propylene: temperature-dependent studies. J Quant Spectrosc Radiat Transf 2014;133:559–69. http://dx.doi.org/10.1016/j.jqsrt.2013.09.019.

[39] Ainetschian A, Frasar GT, Ortigoso J, Pate BH. Contaminated torsional tunneling splittings in five normal-mode vibrations of propene. J Chem Phys 1994;100:729–32.

[40] Silvi B, Labarbe P, Perchard JP. Spectres de vibration et coordonnees normales de quatre especes isotopiques de propene. Spectrochim Acta 1973;29A:263–76.

[41] de Graauw Th, Haser LN, Beintema1 DA, Roelfsema PR, van Agthoven H, Barl L, Bauer OH, Bekenkamp HEG, et al. Observing with the ISO Short-Wavelength spectrometer. Astron & Astrophys 1996;315:L49-L45.

[42] Lacy JH, Richter MJ, Greathouse TK, Jaffe DT, Zhu Q. TEXES: a sensitive high resolution grating spectrograph for the mid-infrared. Pub Astron Soc Pacific 2002;114:153–68.

[43] Kunde VG, Flasar FM, Jennings DE, Bézard B, et al. Jupiter's atmospheric composition from the Cassini thermal infrared spectroscopy experiment. Science 2004;305:1582–6.

[44] Milam SN, Stansberry JA, Sommeborn G, Thomas C. The james webb space telescope's plan for operations and instrument capabilities for observations in the solar system. Publ Astron Soc Pac 2016;128:018001.

[45] Nixon CA, Achterberg RK, Ádámkovics M, Bézard B, et al. Titan science with the james webb space telescope. Publ Astron Soc Pac 2016;128:018007 (23pp).

[46] Flasar F, Kunde V, Abbas M, Achterberg R, Ade P, Barucci A, Bézard B, Bjoraker G, Brasunas J, Calcutt S, Carlson R, Cesarsky C, Conrath B, Coradini A, Courtin R, Coustenis A, Edberg S, Edgington S, Ferrari C, Fouchet T, Gautier D, Gierasch P, Grossman K, Irwin P, Jennings D, Lellouch E, Mamoutkine A, Marten A, Meyer J, Nixon C, Orton G, Owen T, Pearl J, Prange R, Raulin F, Read P, Romani P, Samuelson R, Segura M, Showalter M, Simon-Miller A, Smith M, Spencer J, Spilker L, Taylor F. Exploring the Saturn system in the thermal infrared: the composite infrared spectrometer. Space Sci Rev 2004;115:169–297.

[47] Coustenis A, Achterberg RK, Conrath BJ, Jennings DE, Marten A, Gautier D, Nixon CA, Flasar FM, Teanby NA, Bezard B, Samuelson RE, Carlson RC, Lellouch E, Bjoraker GL, Romani PN Taylor FW, Irwin PGJ, Fouchet T, Hubert A, Orton GS, Kunde VG, Vinatier S, Mondellini J, Abbas MM, Courtin R. The composition of Titan's stratosphere from Cassini/CIRS mid-infrared spectra. Icarus 2007;189:35–62. http://dx.doi.org/10.1016/j.icarus.2006.12.022.

[48] Rothman LS, Gordon IE, Babikov Y, Barbe A, Benner DC, Bernath PF. et al. The HITRAN 2012 molecular spectroscopic database. J Quant Spectrosc Radiat Transf 2013;130:4–50.

[49] Rothman LS, Gordon IE, Barbe A, Benner DC, Bernath PF, et al. The HITRAN 2008 molecular spectroscopic database. J Quant Spectrosc Radiat Transf 2009;110:533–72.

[50] Gordon IE, Rothman LS, Hill C, Kochanov RV, Tana Y, Bernath PF, et al. The HITRAN 2016 molecular spectroscopic database. J Quant Spectrosc Radiat Transfer 2017. doi:10.1016/j.jqsrt.2017.06.038.

[51] NIST Chem Webbook; http://webbook.nist.gov/chemistry. Copyright (C) 1987 by the Coblentz Society; Collection (C) 2009 copyright by the U.S. Secretary of Commerce on behalf of the United States of America. Origin: DOW CHEMICAL COMPANY. Source reference: COBLENTZ NO. 8879 (1964).

[52] Virtual Planetary Laboratory (http://vpl.astro.washington.edu/spectra/fundamentals.htm).

[53] Jacquinet-Husson N, Armante R, Scott NA, Chédin A, Crepeau L, et al. The 2015 edition of the GEISA spectroscopic database. J Mol Spectrosc 2016;327:31–72.

[54] Jacquinet-Husson N, et al. The 2009 edition of the GEISA spectroscopic database. J Quant Spectrosc Radiat Transf 2011;112:2395–445 101016/jjqsrt201106004.

[55] Lide DR, Christensen D. Molecular structure of propylene. J Chem Phys 1961;35:1374–8.

[56] Durig JR, Guirgis GA, Bell S. Torsional spectrum and ab initio calculations for propene. J Phys Chem 1989;93:3487–91.

[57] Buzan EM, Hargreaves RJ, Bernath PF. High resolution absorption cross-sections for propylene in the 3 µm region at high temperatures. Mol Astrophys 2016;3–4:16–20.

[58] Mantz AW, Sung K, Brown LR, Crawford TJ, Smith MAH, Devi MV, Benner DC. Closed-cycle He-cooled absorption cells designed for a Bruker IFS-125HR. In: Proceedings of the First Results between 79 and 297 K 65th International Symposium on Molecular Spectroscopy, Columbus, OH. Ohio State University; 2010.

[59] Sung K, Mantz AW, Smith MAH, Brown LR, Crawford TJ, Devi VM, Benner DC. Cryogenic absorption cells operating inside a Bruker IFS-125HR: first results for $^{13}CH_4$ at 7 µm. J Mol Spectrosc 2010;262:122–34.

[60] Devi VM, Benner DC, Rinsland CP, Smith MAH, Sams RL, Blake TA, Flaud J-M, Sung K, Brown LR, Mantz AW. Multispectrum measurements of spectral line parameters including temperature dependences of N_2- and self-broadened half-width coefficients in the region of the ν_9 band of $^{12}C_2H_6$. J Mol Spectrosc 2010;111:2481–504.

[61] Devi VM, Benner DC, Rinsland CP, Sung K, Crawford TJ, Mantz AW, Smith MAH. Line positions and intensities for the ν_{12} band of $^{12}C^{13}CH_6$. J Mol Spectrosc 2014;301:28–38.

[62] Devi VM, Benner DC, Sung K, Crawford TJ, Yu S, Brown LR, Smith MAH, Mantz AW, Boudon V, Ismail S. Self- and air-broadened line shapes in the $2\nu_3$ *P* and *R* branches of $^{12}CH_4$. J Mol Spectrosc 2015;315:114–36.

[63] di Lauro C, Lattanzi F, Brown LR, Sung K, Mantz AW, Smith MAH. The ν_4, ν_9, ν_{10} and $\nu_6+\nu_{11}$ bands of $^{12}CH_3{}^{13}CH_3$ between 1345 and 1557 cm^{-1}. J Mol Spectrosc 2014;302:36–49.

[64] CRC handbook of chemistry and physics. DR Lide, 92th ed. New York: CRC Press; (2011).

[65] Wlodarczak G, Demaison J, Heineking N, Császár AG. The rotational spectrum of propene: internal rotation analysis and ab initio and experimental centrifugal distortion constants. J Mol Spectrosc 1994;167:239–47.

[66] Coudert LH, Wagner G, Birk M, YuI Baranov, Lafferty WJ, Flaud JM. The $H_2{}^{16}O$ molecule: line position and line intensity analyses up to the second triad. J Mol Spectrosc 2008;251:339–57.

[67] Drouin BJ, Pearson JC, Walters A, Lattanzi V. THz measurements of propane. J Mol Spectrosc 2006;240:227–37.

[68] Pickett HM. The fitting and prediction of vibration–rotation spectra with spin interactions. J Mol Spectrosc 1991;148:371–7.

[69] Toon GC, Farmer CB, Scharper PW, Lowes LL, Norton RH. Composition measurements of the 1989 Arctic winter stratosphere by airborne infrared solar absorption spectroscopy. J Geophys Res 1992;97:7939–61.

[70] Irion FW, Gunson MR, Toon GC, Chang AY, Eldering A. Atmospheric trace molecule spectroscopy (ATMOS) experiment version 3 data retrievals. Applied Optics 2002;41:6968–79.

[71] Sung K, Toon GC, Crawford TJ. N_2- and (H_2+He)-broadened cross-sections of benzene (C_6H_6) in the 7–15 µm region for the Titan and Jovian atmospheres. Icarus 2016;27:438–52 Corrigendum, Icarus 281: 476 (2017).

[72] Toon GC, Blavier JF, Sen B, Margitan JJ, Webster CR, May RD, Fahey D, Gao R, Del Negro L, Proffitt M, Elkins J, Romashkin PA, Hurst DF, Oltmans S, Atlas E, Schauffler S, Flocke F, Bui TP, Stimpfle RM, Bonne GP, Voss PB, Cohen RC. Comparison of Mk-IV balloon and ER-2 aircraft measurements of atmospheric trace gases. J Geophys Res 1999;104:26779–90.

[73] Crawford B Jr. Vibrational intensities: integration theorems. J Chem Phys 1958;29:1042–5.

[74] Breeze JC, Ferriso CC, Ludwig CB, Malkmus W. Temperature dependence of the total integrated intensities. Spectrochim Acta 1965;32:1059–65.